ELSEVIER

In Collaboration with the Royal Netherlands Institute for Sea Research

Journal of Sea Research 51 (2004) 93–107

JOURNAL OF SEA RESEARCH

www.elsevier.com/locate/seares

Rapid wave-driven advective pore water exchange in a permeable coastal sediment

Elimar Precht*, Markus Huettel

Max Planck Institute for Marine Microbiology, Celsiusstrasse 1, D-28359 Bremen, Germany

Received 7 January 2003; accepted 7 July 2003

Abstract

In this study we present in-situ measurements of pore water flow velocities in a coastal sandy sediment (permeability = 3.65×10^{-10} m^2). The advective pore water flows were driven by the interaction of oscillating boundary flows with sediment wave ripples, (amplitude = 7 cm, wavelength = 30 to 50 cm). The measurements were carried out in the Mediterranean Sea at 50 to 70 cm water depth during a phase of very low wave energy (max. wave amplitude = 10 cm). An optode technique is introduced that permits direct pore water flow measurements using a fluorescent tracer. Near the sediment surface (0.5 cm depth) pore water reached velocities exceeding 40 cm h^{-1}. Thus, advective transport exceeded transport by molecular diffusion by at least 3 orders of magnitude. Based on the pore water velocity measurements and ripple spacing, we calculate that 140 L m^{-2} d^{-1} are filtered through the sediment. Pore water visualisation experiments revealed a flow field with intrusion of water in the ripple troughs and pore water release at the ripple crests. The wave-driven water flow through the sediment, thus, was directly linked to the wave-generated sediment topography, and its spatial dimensions. These results show that surface waves cause water filtration through permeable sediments at water depths smaller than half the wavelength. We conclude that surface gravity waves constitute an important hydromechanical process that may convert large areas of the continental shelves into expansive filter systems. Surface gravity waves thereby could affect suspended particle concentration and cycling of matter in the shelf.

Keywords: Permeable sediment; Coastal sand; Advection; In-situ optode; Pore water flow velocity measurements; Surface gravity waves

1. Introduction

In permeable sandy sediments that are common in coastal and shelf environments (De Haas et al., 2002), interaction of boundary layer flow and sediment topography can drive interstitial pore water flows. Such advective transport may be an important link between sediment and water column processes and could affect coastal and shelf biogeochemical cycling as it can exceed transport by molecular diffusion by several orders of magnitude (Webb and Theodor, 1972; Rutgers van der Loeff, 1981; Lohse et al., 1996; Huettel and Webster, 2001).

Webb and Theodor (1968) observed that under moderate wave conditions dyed water injected into a coarse sandy nearshore sediment was drawn to the sediment surface in a matter of minutes. These authors concluded that surface gravity waves were the driving

* Corresponding author.
E-mail address: eprecht@mpi-bremen.de (E. Precht).

1385-1101/$ - see front matter © 2004 Elsevier B.V. All rights reserved.
doi:10.1016/j.seares.2003.07.003

force behind this process, as density-driven and biological processes could be ruled out. Shum (1992) used a two-dimensional numerical approach to calculate the trajectories of pore water particles under a rippled bed over one wave period. The results indicated that the zone of advection extended to a few ripple heights below the ripple surface over a wide ange of wave conditions and sediment characteristics. Advective exchange driven by surface gravity waves was quantified in a series of laboratory wave tank experiments by Precht and Huettel (2003). These authors also showed that wave-induced pore water exchange increased sharply at the temporal transition from a smooth to a rough sediment surface when ripples were generated by the oscillating boundary flows.

The term 'subtidal pump' for the exchange between sediment and water column driven by wave-related hydrostatic pressure oscillations was introduced by Riedl et al. (1972). These authors used in-situ data to calculate the amount of water forced through the bed and concluded that the subtidal pump could filter the global ocean volume through the shelf sediments in ca. 14 000 years. Rutgers van der Loeff (1981) described the effect of wave pumping in intertidal flats and concluded that observed increased solute flux was caused by pore water exchange driven by waves. In order to explain net transport of solutes by periodic interstitial motion, the concept of mechanical dispersion was added to the subtidal pump theory (Harrison et al., 1983). In a numerical and experimental approach, Webster and Taylor (1992) showed that dispersion driven by surface gravity waves was able to enhance the solute transfer between sediment bed and overlying water and introduced the term rotational dispersion. Precht and Huettel (2003) proposed that wave-driven exchange at water depths $<$ wavelength/2 caused by oscillating flow-sediment topography interaction may exceed the effects of wave-pumping at least by a factor of 3.

These wave-induced transport processes may cause characteristic changes in the biogeochemical zonation of permeable sediments. Shum's (1993) model calculations indicate that the oxygen distribution in the pore water underneath a rippled surface under progressing waves can display horizontal concentration gradients that may be of the same order of magnitude as those in the vertical direction.

Advective exchange processes driven by unidirectional near-bottom flows have been studied in more detail than exchange driven by oscillating currents. Thibodeaux and Boyle (1987) and Savant et al. (1987) investigated the flow patterns in permeable sediment generated by obstructions on the sediment surface. Advective solute exchange was studied and quantified for a streambed with bedforms and nonsorbing solutes (Elliott and Brooks, 1997a,b); a rippled bed and adsorbing metals (Eylers et al., 1995); biogenic sediment structures and nonsorbing solutes (Huettel and Gust, 1992) and solid obstacle-boundary flow interactions (Hutchinson and Webster, 1998). The biogeochemical implications of advection were examined by Ziebis et al. (1996) for oxygen penetration depth, and by Huettel et al. (1998) for biogeochemical reaction zones in permeable sediments. With interfacial water exchange, suspended particles (Huettel et al., 1996) or phytoplankton (Huettel and Rusch, 2000) locally can be transferred from the boundary layer into the top centimetres of permeable sediments. Thus, the classical one-dimensional approach developed for describing the distribution of pore water constituents and for measuring the related fluxes across the sediment-water interface is inadequate for permeable shelf beds that permit pore water flows (Shum and Sundby, 1996).

The aim of the present study was to gather in-situ data on advective exchange driven by oscillating flow – ripple interaction, and to compare the results with the findings of laboratory studies and model calculations. A method to directly measure pore water velocities in a natural environment and its application to facilitate estimates of the magnitude of advection and its filtering effects is presented. Additionally, a method permitting the visualisation of the evolving pore water flow patterns was applied and is presented.

2. Methods

2.1. Study site

Pore water velocity measurements and pore water flow field visualisations were carried out in October 2001 in shallow-water sediments of Campese Bay at the western coast of the Island of Giglio. Giglio is part of the Tuscany Archipelago in the Mediterranean

Sea off the western coast of Italy, approximately 150 km north-west of Rome at 42°20′ N, 10° 52′ E (Fig. 1). The tidal regime is microtidal as in the whole Mediterranean Sea. The beach and sublittoral of Campese Bay consist of permeable medium sand with a high content of Pyrite grains as iron ore was mined on Giglio and washed and loaded in Campese Bay until ca. 1950. In the shallow (< 10 m) areas of the bay, surface gravity waves produce wave ripples parallel to the coast, while in the deeper regions mounds created by the burrowing activity of the mud shrimp *Calianassa truncata* are the main topographical features (Ziebis et al., 1996). Due to the calm weather conditions prior to the measurement campaign, the *Calianassa* activities had largely destroyed the regular wave ripple pattern in the areas deeper than 2 m. Salinity during the measurement period was 39, water temperature ca. 22 °C and weather conditions were calm with wind velocities of 2 to 5 m s^{-1}. The measurements were carried out in sediment at 50 to 70 cm water depth. This shallow depth was chosen as only small waves were present. Symmetric wave ripples dominated the sediment topography at the study site with amplitudes between 6 and 8 cm and wavelengths between 30 and 50 cm. Although rolling sand grains could be observed at the ripple crests, the ripples as such remained stationary during the measurements.

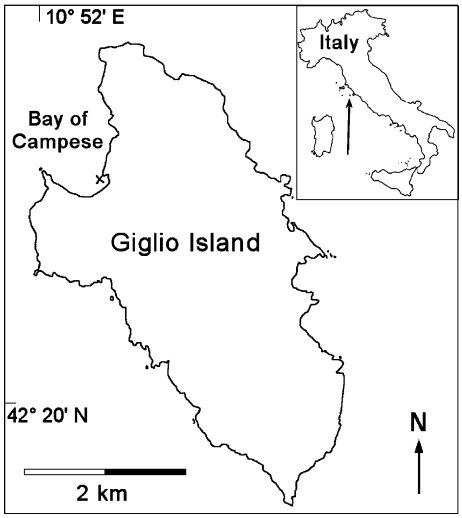

Fig. 1. Bay of Campese, x indicating study site.

The grain size distributions in the sediment surface layer (0–5 cm) were different at the ripple troughs and crests, with median values of 370 μm and 500 μm for the crests and troughs, respectively. The higher median value for the troughs was mainly due to a slight accumulation of gravel (max. diameter: ca. 1 cm) in the ripple troughs. This had no significant influence on permeability and porosity, which were 3.65×10^{-10} m^2 (sd = 1.64×10^{-10}, n = 4) and 36.9 % (sd = 1.35, n = 10), regardless of where the sediment cores for these measurements were taken.

2.2. Water column hydrodynamics

The wave heights were measured with a pole fitted with a scale that was anchored in the sediment at the study site. Water currents were measured using an Acoustic Doppler Velocimeter (Nortek). The ADV technique allows 3 component current measurements in a small measuring volume located ca. 10 cm below the sensor. Two time series of triplicate flow measurements were carried out; one set above a ripple crest, one above a trough. The downwards measuring ADV sensor was attached to a custom-built aluminium frame with a transverse system permitting us to move the measuring volume vertically to predefined specific depths (27, 15, 5 cm and 30, 19, 5 cm above the sediment surface at crest and trough, respectively). Flow velocities were recorded at each measuring point for 1000 s with a sampling frequency of 25 Hz.

2.3. Pore water flow measurements

The measurements of the pore water flow velocities were carried out by injecting 2 ml of fluorescent dye into the sediment and subsequently following the movement of the dye cloud through the sediment with optical sensors. The dye was a Fluorescein solution (100 mg L^{-1}) with a density attuned to the local seawater by addition of NaCl to neutral buoyancy.

The principle of detection of a fluorescent solution with optical fibres is similar to that of oxygen measurements with optodes as laid out by Klimant et al. (1995). De Beer and Schramm (1999) employed this technique of detection of a fluorescent dye with an optical fibre to measure convective transport in a biofilm. For Fluorescein concentration measurements, blue light (λ = 470 nm) is emitted through an optical

fibre into the measuring medium where the light causes excitation of the Fluorescein. The resulting fluorescence signal is transferred back through the same optical fibre, and the intensity is measured after passage through a green interference filter ($\lambda = 519$ nm) with a photo-multiplier tube (PMT). The intensity of the signal is linearly proportional to the Fluorescein concentration within the range of the dye concentrations employed (F. Janssen, unpubl. data). A custom-built fibre optical switch with 7 channels allowed connecting 6 optical fibres for fluorescence measurements and one internal reference. The electronics were housed in a sealed titanium cylinder, and power was supplied by a submergible 24 V battery. The cylinder containing the electronics and the battery were placed onto the sediment 3 m away from the actual measuring site ensuring no interference with the measurements. Prior to the measurements, thermal equilibrium of the electronics with the surrounding water was allowed, as the PMT gain is temperature sensitive. A cable connection allowed the direct surveillance of the measured data with a laptop computer on the beach.

The optical fibres (Radiall; fibre diameter = 140 μm) were stripped of their outer elastic plastic coating but retained their inner plastic cladding for protection resulting in a sensor tip diameter of < 1 mm. The ends of the fibres were cut straight to achieve an optimal compromise between sturdiness and signal strength.

The fluorescence sensors were fixed in an array that was constructed from mesh wire (mesh width 1.25 cm). This set-up allowed aligning the sensors in a 'comb' with 1.25 cm vertical distance between the sensor tips (Fig. 2). A hypodermic needle was attached to the array 2.5 cm below and parallel with the lowest sensor tip. The end of the needle was vertically aligned with the sensor tips. The shaft of the needle was connected with tubing to a syringe that permitted release of a defined tracer volume through the buried open end of the needle. With this set-up, the optical sensors and the hypodermic needle could be placed at fixed and known positions in the sediment covering a distance of 8.75 cm. For the measurements, the array was positioned vertically in the centre of the ripple crests parallel to the ripple geometry. The uppermost fluorescence sensor was ca. 1 mm below the sediment surface at the ripple crests so that the dye was injected ca. 8.8 cm below the sediment surface. The sensor

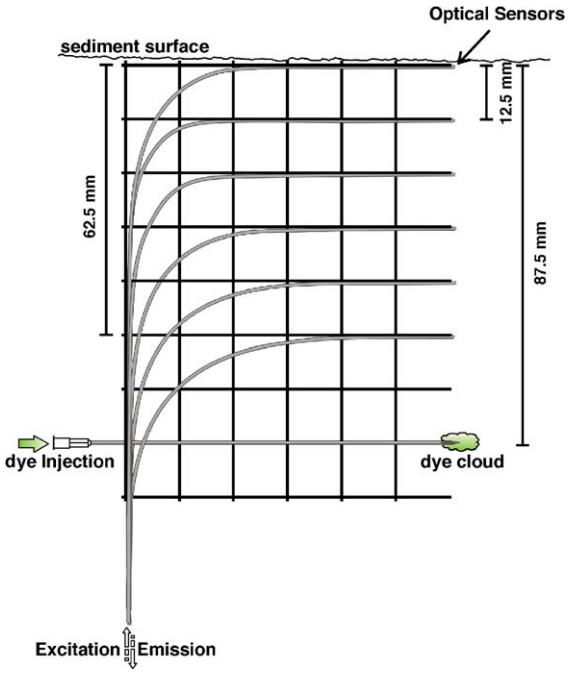

Fig. 2. Sketch of the set-up of the optical sensors: grey are the optical fibres, black the mesh wire framework.

array was inserted into the ripple manually by partially removing the ripple, pressing the array horizontally into an undisturbed part of the ripple and rebuilding the ripple where it had been disturbed. Thus all measurements were carried out in undisturbed parts of the ripples. After injection of Fluorescein, the passage of the dye cloud past the optical sensors could be recorded in the measurements. Four successful measurements of dye migration in the sediment were carried out, two of them with three successive dye injections. The bulk flow velocity of the pore water could then be inferred from the time between the passages of the Fluorescein concentration maxima at the individual optical sensors.

2.4. Pore water flow visualisation

The temporal distribution of a dye cloud in the sediment in order to assess the pore water flows could be visualised in-situ with a simple technique: a 20 cm wide and 30 cm long transparent polycarbonate plate (6 mm thick) was carefully pushed vertically into the sediment perpendicular to the ripples and thus aligned

with the main boundary flow. By removing the sediment on one side of the plate, the cross-section of the ripple became visible. The plate had silicone-sealed holes (0.5 cm in diameter) drilled at regular intervals in a rectangular grid pattern. Through these holes, dye could be injected into the sediment with a hypodermic needle, and additionally these holes served as reference points. The dyes employed for these pore water flow visualisations were neutrally buoyant and thermally equilibrated Rhodamine or Fluorescein solutions. The movement and development of the dye cloud in the sediment could be observed visually through the transparent sheet and for quantitative analyses was recorded with an underwater digital camera. The camera was attached to a custom-built aluminium frame anchored in the sediment and photographs were taken at regular time intervals.

2.5. Sediment characteristics and pore water analyses

At the study site, 3 sediment samples were taken at ripple crests and 3 in the ripple troughs. Each sample consisted of surface sediment (top 5 cm of the sediment) and comprised about 500 g of dry material, which was used to assess grain size distributions using a column of 8 sieves.

To assess the porosity, 5 + 5 sediment cores (diameter: 2.6 cm, length: 3.3 to 9 cm) were taken at ripple troughs and crests. Supernatant water was carefully removed, and the cores were sealed and stored for transport. The porosities of the respective cores were calculated from the wet and dry (after drying at 50 °C to constant weight) weights and corrected for salinity.

For permeability measurements, 4 sediment cores (diameter: 2.6 cm, length between 8.5 and 13.7 cm) were taken at both ripple crests and ripple troughs. Measurements were done directly after sampling with a constant head permeameter (Klute and Dirksen, 1986).

For nutrient analyses, pore water was extracted using a steel pore water sampler with a perforated pointed tip filled with filter material. 3 × 3 samples were taken 10, 20 and 30 cm below both ripple troughs and crests (ca. 4 to 5 ml each). According to the measured porosities, pore water was extracted from a sediment volume of ca. 13.5 cm^3, which means a vertical resolution of ca. 3 cm assuming a spherical shape of the extracted water volume. These 18 pore water samples and 3 open water samples were preserved with 0.1 ml of $HgCl_{2\ sat.}$ solution directly after retrieval, sealed and stored for nutrient analysis. The samples were diluted by factor of 3 and analysed spectrophotometrically for NO_3^-, NO_2^-, NH_4^+, PO_4^{3-} and $Si(OH)_4$ with a Scalar 5-canal Continuous-Flow-Auto-Analyser. The chemistry of the underlying reactions is described in Grasshoff et al. (1999). Pore water salinity was measured in the same samples.

Sediment temperature measurements were carried out with temperature loggers (HOBO, resolution = 0.7 °C) at various sediment depths down to 20 cm.

3. Results

3.1. Flow measurements in the water column

Wave conditions during the entire measurement period were calm with wave amplitudes not exceeding 10 cm. A power spectrum analysis of the ADV data revealed a distinct peak at 0.18 Hz, implying a main wave period of 5.5 s. Wave amplitude was 6 cm during the ADV measurements, and this wave action was not strong enough to induce ripple migration. Only motion of very few sand grains at the ripple crests could be observed. An excerpt representative of the measurements and the conditions during the study period is shown in Fig. 3. The dominant water motion 27 cm above the ripple crest was the horizontal oscillation perpendicular to the crests with maximum velocities of 30 and −30 cm s^{-1}, whereas maximum vertical velocities reached 10 cm s^{-1} and −10 cm s^{-1}. The averaged orbital velocities were 9.8 cm s^{-1} and 9.2 cm s^{-1} at 27 cm and 15 cm above the ripple crests, respectively. The RMS values for the main horizontal velocity component at these depths were 9.7 and 8.5 cm s^{-1}, respectively.

3.2. Pore water flow field

The motion of the pore water tracer in the sediment could directly be observed through the transparent panes inserted into the sand bed. Tracer injection at different locations under the ripple

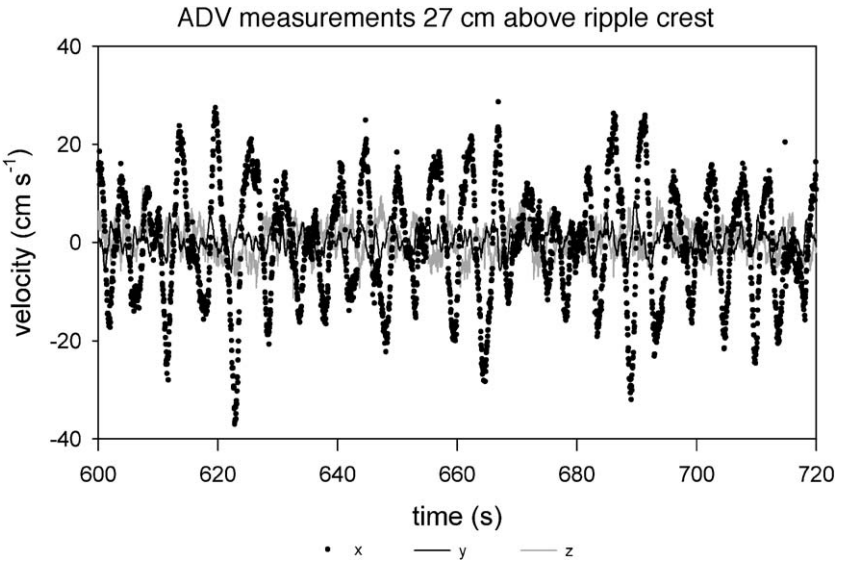

Fig. 3. Excerpt from one of the ADV measurements.

revealed the local pore water flow pattern, and the sum of all observations gave an image of the pore water flow field.

After injection of a dye cloud (2.5 cm diameter) directly underneath the ripple crest at 6 cm sediment depth, the dye migrated vertically upwards and finally emerged from the sediment at the ripple crest. The upwelling dye cloud became horizontally compressed and vertically elongated on its path to the ripple crest. (Fig. 4a).

Injection of dye to 1 cm sediment depth into the land- and seaward slopes of the ripples resulted in sideways dye movement along a curved path towards the ripple crest, where it finally emerged from the sediment (Fig. 4b).

Injection of dye into the centre of a ripple trough showed the dye cloud propagating downwards and simultaneously being stretched towards the ripple crests, with the first dye release at the ripple crest after 30 min (Fig. 4c).

The pore water flow field that could be reconstructed from these observations is schematically depicted in Fig. 5. Water enters the sediment in the ripple troughs and at the ripple flanks and

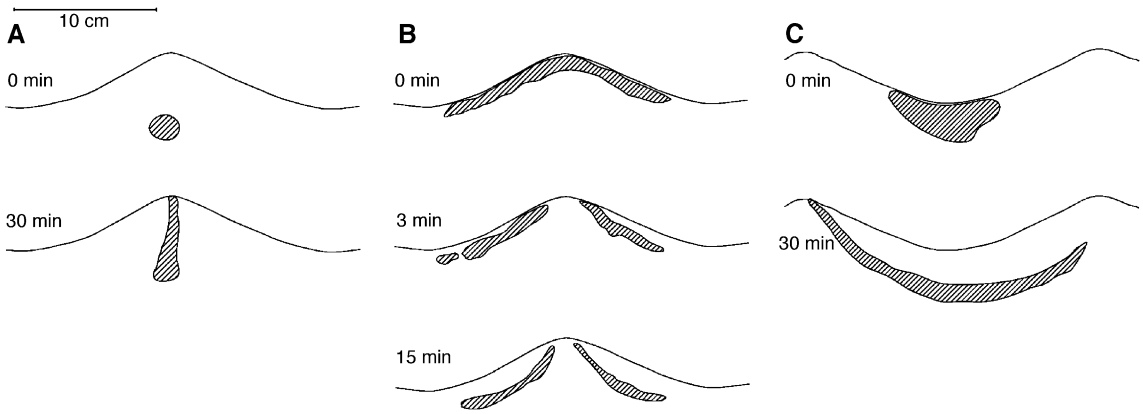

Fig. 4. a–c. Sketch summarising the results of the pore water flow field dye experiments.

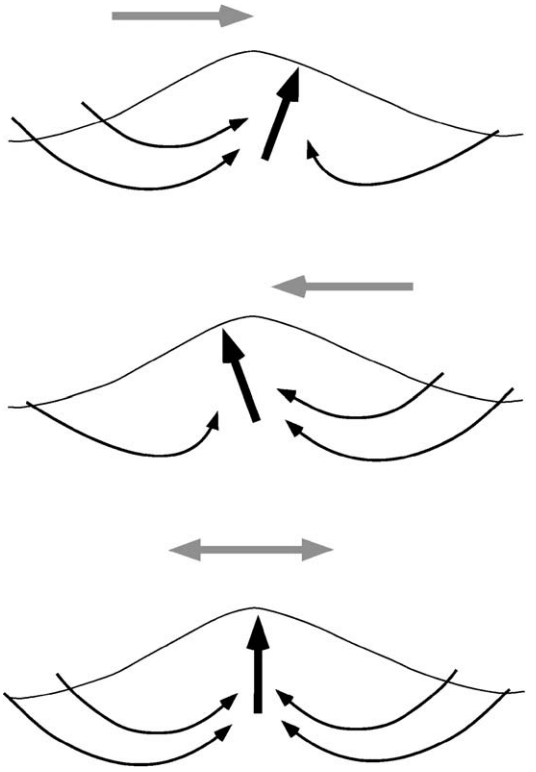

Fig. 5. Schematic overview of pore water flow field driven by oscillating flow interacting with a sediment ripple. Top and centre show the pore water flow field that would develop under steady unidirectional flow in opposing directions; the bottom drawing shows the averaged pore water flow field under oscillating flow as induced by surface gravity waves.

leaves the sediment centred at the ripple crests. This pattern evolves as the average of the two pore water flow fields that would evolve under unidirectional flows in opposing directions. The seawater penetrating into the sediment close to the ripple crest follows a short path to the ripple crest and passes the sediment relatively fast and close to the sediment surface. Water penetrating in the centre of the troughs reaches deeper zones of the sediment, but all filtered water leaves the sediment through the emergence zone, a band comprising the central area of the ripple crest. Using the pore water flow field images, the lengths of the pore water pathways could be estimated, which, in the upper 10 cm of the sediment, ranged from 10 to 31 cm (average: 17.5 cm).

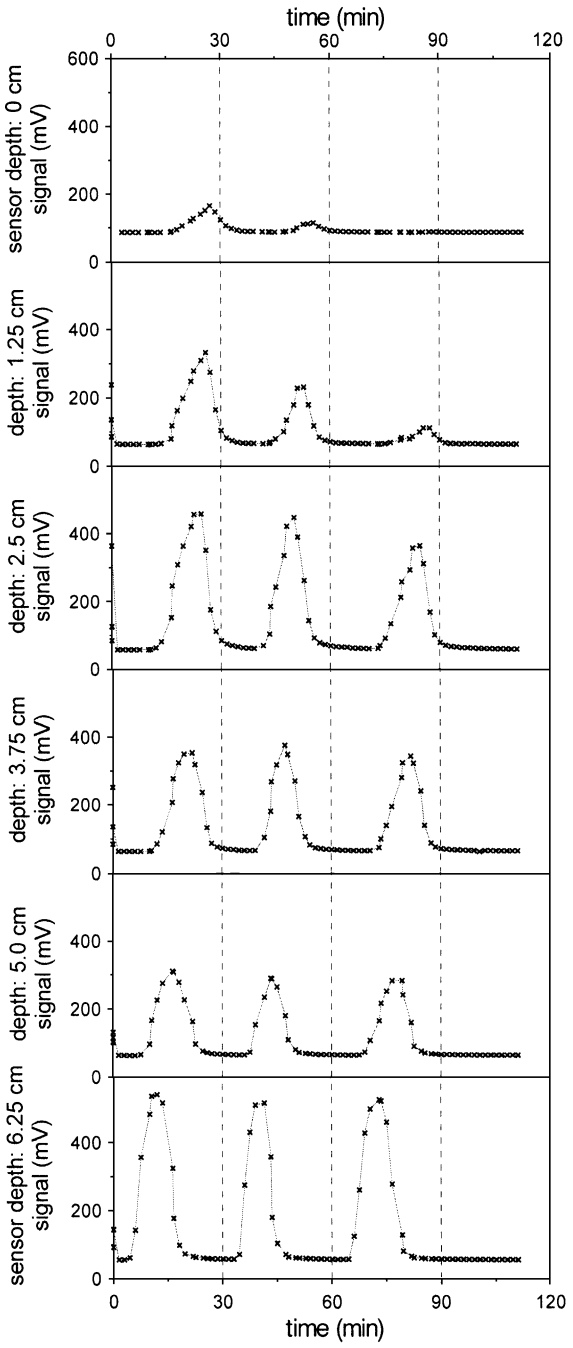

Fig. 6. Result of pore water velocity measurements: example with 3 successive dye injections passing the sensors on their path to the ripple crest.

3.3. Pore water velocity

The pore water velocity measurements were conducted in the upwelling zone along a vertical line directly underneath the ripple crests. In all measurements, the tracer cloud passed by the optical sensors and created distinct peaks in the sensor signal. This is presented in Fig. 6, which shows the results of an experiment with three sequential dye injections. The results of all other experiments looked similar. The matrix-averaged pore water velocity is the bulk velocity at which the tracer cloud moves through the sediment. It can be calculated from the distance of the signal peaks. The upward bulk velocity between 0 and 6.25 cm depth averaged over all valid measurements was 26 cm h^{-1} (sd = 16.2, n = 36). Fig. 7 shows a plot of the averaged vertical pore water velocities versus depth. It can be seen that the velocity decreased with depth with values ranging from >40 cm h^{-1} between the uppermost sensors to 21 cm h^{-1} between the lowest sensors.

3.4. Pore water characteristics

The nutrient concentrations did not change significantly in the pore water samples taken at 10, 20 and 30 cm depth and were not significantly different from the nutrient concentration in the overlying water except for silicate. No accumulation of NO_3^-, NO_2^-, NH_4^+ or PO_4^{3-} in these layers could be detected.

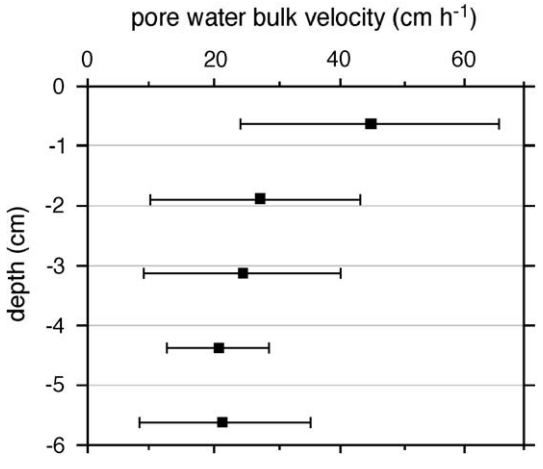

Fig. 7. Upward pore water velocity underneath ripple crest at various depths.

$Si(OH)_4$ was detectable with 11 μM (sd = 4, n = 18) in the pore water and 2.4 μM (sd = 0.12, n = 4) in the water column. The pore water solute concentrations were very low with measured concentrations of NO_3^-, NO_2^-, NH_4^+ and PO_4^{3-} around or below the detection limit of 0.3 μM in the pore water and water column samples.

Pore water salinity was ca. 39 and uniform over depth in the upper 30 cm of the sediments. Likewise, sediment temperature was 21.5 °C down to 20 cm and showed no significant variations at the resolution of the sensors.

4. Discussion

In this study, we present direct in-situ measurements of interstitial flow velocities in permeable coastal sediment. The measurements reveal that even weak wave action can produce rapid and effective pore water exchange in shallow permeable beds. In the sediments investigated, pore water velocities of almost 1 cm min^{-1} were reached near the sediment water interface.

The optode technique proved to be a useful method for measuring the pore water velocities in-situ without disturbing the sediment structure. The optodes were embedded in the sediments such that pore water flow velocities were measured only in undisturbed sections of the ripples, and the thin optodes did not create additional pathways for pore water. A possible local sediment compaction caused by the optode insertion would reduce sediment permeability and therefore lower pore water flow velocities. While pore water velocities could be determined from the passage of concentration peaks by the sensor tips, a quantitative analysis of the dye concentration in the pore space was not possible. The strength of the fluorescence signals was not only dependent on the dye concentrations but also on the pore space geometry in front of the optical sensor, possible mechanical damage to the sensor tip or fouling. Efforts to calibrate the sensors in-situ to obtain quantitative data on dye concentrations were unsuccessful, which did not affect pore water velocity measurements but excluded assessment of phenomena such as dispersion. Moreover, it can be inferred from Fig. 6 that the intensity of the fluorescence signals decreased at the upper mea-

suring ports. This is probably due to the sensor array not being perfectly aligned with the pathway of the dye cloud. The dye cloud, which is narrowed on its path to the sediment surface, then passes the upper sensors not centrally causing a weaker signal. Other explanations may be dispersion or longitudinal advection caused by imperfectly aligned ripples and waves. The weak signal at the uppermost sensor may also be caused by minor grain migration on the ripple crests in the measurements with multiple injections, thereby exposing the sensor.

Injection of the dye into the sediment produces a pressure gradient that will drive pore water flow. This temporal artificial pressure gradient will not affect the measured pore water velocities, as these are measured well after the injection by inferring the velocity from the passage of the peak of dye concentrations at the single sensors.

The transparent acrylic plates inserted into the sediment for pore water visualisation were more likely to affect the results because sections of the plates sticking out of the sediment could obstruct the flow. This effect could be minimised by placing the plates perpendicular to the main direction of the oscillating flows. However, the technique only allows the visualisation of flow directly adjacent to the acrylic plate. Therefore wall effects that may reduce the pore water velocity near the plate could not be excluded. Additionally, the missing part of the ripple may have an influence on the pore water flow. Nevertheless, this technique produced reproducible results that were consistent with the optode measurements and the findings of previous studies suggesting that the artefacts linked to the wall effect were relatively small.

Pore water flows in permeable beds can be caused by a number of different processes, and in the following we discuss how these processes may have affected our observations. Interstitial water motion close to the swash zone can be linked to beach drainage after swash run up (Riedl and Machan, 1972). Waves running up the beach could theoretically cause pore water motion as far away from the beach as where our measurements were carried out. This beach groundwater ideally flows on curved pathways through the beach back into the sea (Longuet-Higgins, 1983; Li et al., 1999). On a larger time scale, also tidal dynamics may drive beach drainage (Nielsen, 1990). Neither process could explain the observed flow pattern within the ripple. Furthermore, the swash zone only spanned a few centimetres during the measurements and the study site is microtidal.

Density-driven convection due to salinity or temperature differences is another possible mechanism to drive interstitial flows (Webster et al., 1996; Rocha, 2000). As the salinity measurements in the upper 30 cm of the sediment and the temperature measurements in the upper 20 cm showed no variability, this mechanism can be ruled out as driving force for the pore water flow patterns observed in this study.

The recorded pattern of water entering the sediment in the ripple troughs and emerging from the sediment at the ripple crests is in very good agreement with the observations of Webb and Theodor (1972) after in-situ dye injection – reappearance experiments and the model calculations by Shum (1992). In contrast to unidirectional flows that cause upwelling of fluid under the downstream slope of sediment ripples (Huettel and Gust, 1992; Huettel et al., 1996), wave-induced oscillating flows can produce a symmetric pore water flow pattern relative to the sediment ripples as the strength of the flow is similar in both directions (Fig. 5). The water penetrating on both sides of the ripple and the acceleration of the pore water close to the sediment surface result in a narrowing and focusing of the centrally upwelling pore fluid. This flow field characteristically reduces mixing of the pore water moving from deeper sediment layers towards the surface.

With the measured averaged pore water velocity of 26 cm h^{-1} under the ripple crests (upper 6.2 cm), solutes in the pore water can effectively be transported over a distance of 1 cm in less than 3 min. The time it would take a solute to travel this distance by molecular diffusion can be approximated by $t = z^2 / 2D$ with t, z and D denoting time (s), distance (cm) and diffusion coefficient in water ($cm^2\ s^{-1}$), respectively. The span of biogeochemically relevant D values for ions, gasses and molecules in water ranges from 0.4 to 2×10^{-5} $cm^2\ s^{-1}$ (Jørgensen, 2001). For oxygen in seawater with a salinity of 39 and a temperature of 22 °C, the diffusion coefficient is 2.07×10^{-5} $cm^2\ s^{-1}$ (Li and Gregory, 1974). In the sediment, the tortuosity of 2.99 (Boudreau, 1996) has to be taken into account to assess the sediment's effective diffusion coefficient, which is, calculated after Boudreau (1996), 2.55×10^{-6} $cm^2\ s^{-1}$. Using these values in the above

equation shows that diffusive transport of oxygen would need ca. 54 h to overcome the distance of 1 cm in our sediment. Advective oxygen transport in our sediments due to the wave-topography interaction thus is more than three orders of magnitude faster than transport by diffusion alone.

A tortuosity of ca. 3 implies that the actual velocity of water flowing through the sediment's pore space is three times faster than the bulk velocity of a several centimetre wide solute cloud moving through the sediment. Under the ripple crest, this matrix-averaged velocity ranged from >40 cm h^{-1} close to the surface to 20.5 cm h^{-1} between 6.2 and 5 cm depth. The typical directional swimming velocity of a bacterium lies in the order of 2 μm s^{-1} (Jørgensen, 2001), which equals ca. 1 cm h^{-1}. This value is 60 to 120 times lower than the interstitial velocities we measured corrected for tortuosity, which may explain why more than 90% of the bacterial cells in surface layers of permeable sea beds are attached to the mineral grains (Rusch et al., 2001).

The resulting rapid advective pore water exchange in the upper sediment layers is reflected in the uniform pore water nutrient profiles showing values around or below the detection limit. Only $Si(OH)_4$ displayed slightly elevated but uniform values in the sediment compared to the overlying water.

In combination with the uniform pore water salinity and sediment temperatures, these findings indicate that at least the upper 30 cm of the sediment were completely and constantly flushed, linking pore water concentrations tightly to the solute concentrations in the overlying water column. Constant flushing of the sediment causes at least the upper 20 to 30 cm of the sediment to be in thermal equilibrium with the overlying water.

The upward pore water velocity under the ripple crests can additionally be used to assess the filtering rates of water through the sediment because the only areas where pore water was released from the sediment were the ripple crests: with an average distance of 40 cm between neighbouring ripple crests, the total length of ripple crest per m^2 of sediment surface at our study site was approximately 250 cm. Multiplied by the averaged pore water upwelling velocity of 26 cm h^{-1} underneath the ripple crests, an average width of the release zone of 2.5 cm and the porosity of 36.9 %, this results in a filtering rate of ca. 140 L m^{-2} d^{-1}.

Advective filtering leads to enhanced transfer of suspended particles (Huettel et al., 1996) or phytoplankton (Huettel and Rusch, 2000) into the sediment. During the measurement campaign, the particulate organic carbon (POC) content in the water column of Campese Bay was approximately 0.4 mg C L^{-1} dry mass (C. Wild, unpubl. data). Assuming complete filtering of the particulate matter in the sediment, the filtering rate we assessed suggests that at the study site ca. 50 mg m^{-2} d^{-1} particulate organic carbon could be carried into the sediment by this wave-induced exchange process. This is in the same range as the findings of Durrieu De Madron et al. (2000), who found between 16 and 24 mg m^{-2} d^{-1} particulate organic carbon deposition on the shelf of the Gulf of Lions in the Mediterranean. Canfield and Teske (1996) calculated a median carbon oxidation rate of 164 mg m^{-2} d^{-1} for modern coastal sediments in water depths <200 m from the findings of 60 studies. As 87.5 to 97% of the carbon deposited at the seafloor is decomposed (Berger et al., 1989), our values are in the same order of magnitude but smaller, which can be attributed to the oligotrophic conditions in the Mediterranean.

4.1. Comparison with other studies

To our knowledge, very few studies have dealt with in-situ measurements of wave-induced transport processes. Webb and Theodor (1968, 1972) worked at 3 m water depth under waves producing stronger bottom boundary flow than in this study. The sediment at their study site was coarser (median ca. 1000 μm) and thus more permeable. Calculations of filtering rates based on their estimates for pore water velocity (average 130 cm h^{-1}) underneath the ripple crests result in an average filtering rate of ca. 300 L m^{-2} d^{-1} (assuming a conservative release area width of 2 cm and a porosity of 37%). This value is larger than our findings, due to the different wave and sediment characteristics, but lies well within the range of this study.

Compared to the findings of Riedl et al. (1972), who investigated wave pumping on the North Carolina Shelf, our results suggest a filtering rate that is 3 to 4 times larger and deeper penetration of the advective flows into the sea bed. The sediments

Riedl et al. (1972) examined were slightly finer (250 to 177 μm mean grain diameter) but this may have been partly compensated by the stronger wave action present during their field experiments. The magnitude of the filtration rates we calculated from the in-situ measurements is also supported by wave tank experiments of (Precht and Huettel, 2003), which were carried out with a finer, less permeable sediment and smaller ripples than in Campese Bay but resulted in a filtering rate larger or in the same range as in this study (60 to 590 L m^{-2} d^{-1}).

Interstitial flow induced by unidirectional currents was studied in the laboratory by Savant et al. (1987). These authors employed sand with a mean particle diameter of 370 μm, and a flow of 20 cm s^{-1} over ripples of 5 cm height and 50 cm wavelength. Thus, the physical parameters were comparable to those we found at our study site. These authors observed porewater flow velocities between 3.2 cm h^{-1} and 26.3 cm h^{-1}. This demonstrates that advective porewater motion induced by oscillating and unidirectional flow lies in the same order of magnitude.

The filtering rates calculated from measurements can be compared to the rates derived from the analytical model of Elliott (1990) that gives the pressure perturbation p created by a sediment ripple interacting with unidirectional flow as:

$$p = 0.14\rho u^2(\delta/0.34H)^{3/8} \quad (1)$$

For $\delta/H \leq 0.34$ and with ρ, u, δ and H denoting density, mean current velocity, ripple height and water depth, respectively. From the pressure perturbation, the flow volume per area can be calculated:

$$w_0 = (2k/\rho\nu L_D)p \quad (2)$$

With k, ν, and L_D denoting permeability, kinematic viscosity and decay length (= the length scale of the ripple), respectively (Huettel and Webster, 2001). Using the measured values ($u_{RMS} = 0.09$ m s^{-1}; $\delta = 0.07$ m; $k = 3.65 \times 10^{-10}$ m^2; $L_D = 0.40$ m and $\nu = 1.024 \times 10^{-6}$ m^2 s^{-1} (calculated after Krögel, 1997), this results in a mean pressure perturbation of 1.05 Pa, which yields a theoretical flushing rate of 158 L m^{-2} d^{-1}. This is in very good agreement with our measured values.

The findings of previous studies on the magnitude of solute transport driven by different processes in the sediment are summarised in Fig. 8. Fig. 9 shows the ensuing filtering rates of water through permeable sediments and reveals that wave-driven advective pore water flow and filtering substantially exceed the magnitude of other wave-driven transport processes, with the exception of swash in- and exfiltration. The latter, however, has only a very limited spatial extent. The pore water velocities under unidirectional flow are similar to those we found in this study, so it is likely that filtering rates can reach higher values than those reported so far.

4.2. Applicability of data on a broader scale

In this study, we describe advective pore water exchange driven by the interaction of oscillating boundary flow with sediment topography rather than wave-related hydrostatic pressure oscillations. Webb and Theodor (1968) showed that these processes also occur in slightly deeper water. Wave-driven advection can take place in extended areas of the global shelves covered by permeable sediments with water depths < wavelength/2. Here, oscillating currents are generated at the seafloor, which then interact with the sediment topography. The magnitude of the advective pore water exchange depends on sediment permeability, bed topography and near-bottom flow velocities.

Many of the sediments of the global shelf seas consist of coarse-grained relict sediments (Emery, 1968) and a wealth of studies have described the abundance of sands and wave ripples on the continental shelves for a variety of study sites and water depths (e.g. Cacchione et al., 1999; Li and Amos, 1999). The study of Black and Oldman (1999) carried out on the Australian and New Zealand Shelf showed that the sediment parameters at our study site can also be found in deeper shelf areas. These authors describe a 20 km wide zone between 20 and 45 m water depth with grain sizes of 300 to 900 μm and ripple wavelengths ranging from 30 to 100 cm, which is close to or larger than the values we found in Campese Bay. The similar sediment characteristics indicate that the hydrodynamic forcing at the seabed may be comparable at both study sites, suggesting that the magnitude of probable advective processes would also be similar. Taking the 20 km wide zone between 20 and 45 m water depth into account and assuming a filtering rate of 140 L m^{-2} d^{-1}, each 1 km of shelf could filter slightly more than 1 km^3 a^{-1} of water

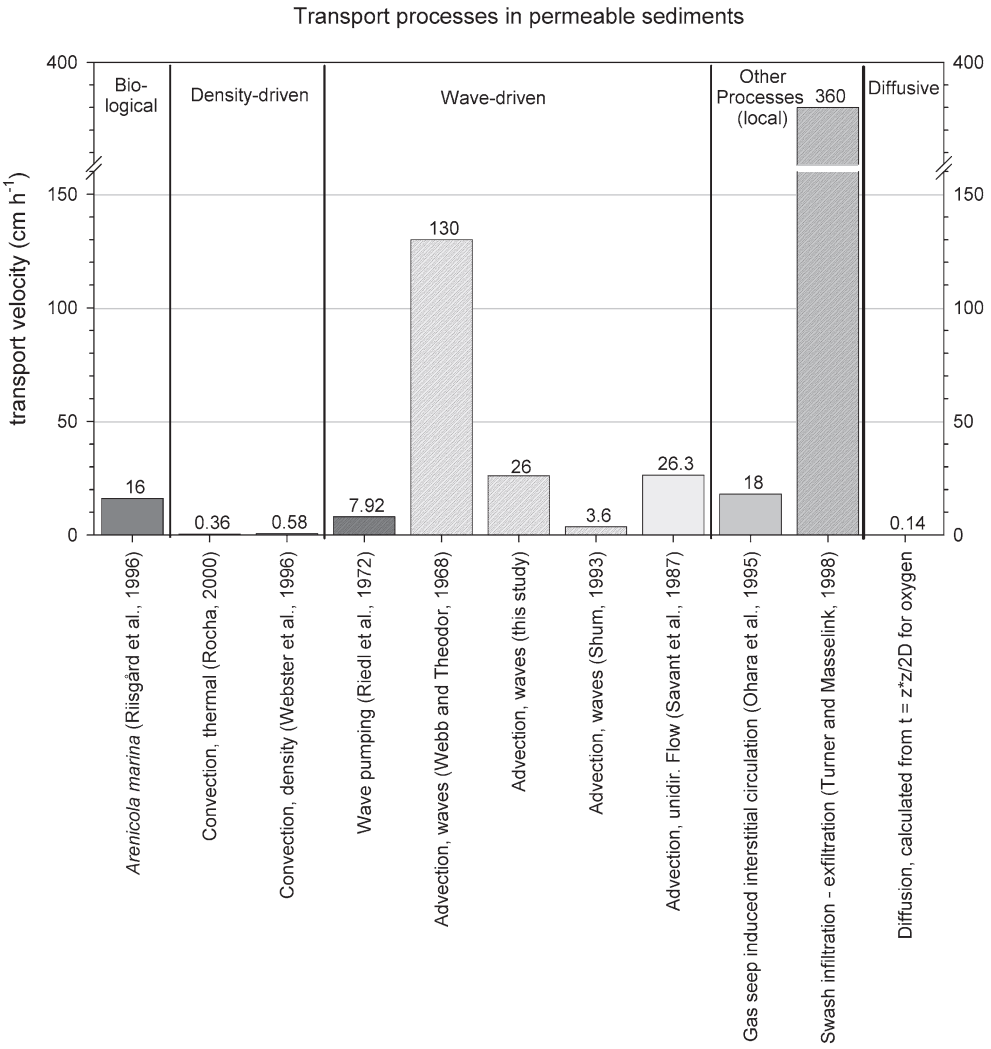

Fig. 8. Comparison of transport velocities in permeable sediments driven by different processes (Riisgård et al., 1996; Ohara et al., 1995; Turner and Masselink, 1998).

through its sediments in this zone alone. This value is considerably larger than the value of 0.419 km^3 a^{-1} of filtering by wave pumping that Riedl et al. (1972) assume for 1 km of an averaged global shelf transect from the beach to the 200 m isobath. This indicates that wave-driven advection is an important mechanism for the interfacial exchange of water, solutes and suspended particles in shallow shelf and coastal environments.

We conclude that for a given sandy coastal sediment with typical permeability, the bulk pore water velocities due to wave-driven advection we measured in-situ lie in the same order of magnitude (several cm h^{-1}) as those driven by advection due to unidirectional flows. The observed wave-driven advection was at least 3 orders of magnitude faster at our study site than solute transfer by diffusion would have been. In shallow coastal environments, the pore water velocities and filtering rates caused by wave induced oscillating boundary flows interacting with sediment topography substantially exceed other wave-driven transport processes. The ecological significance of

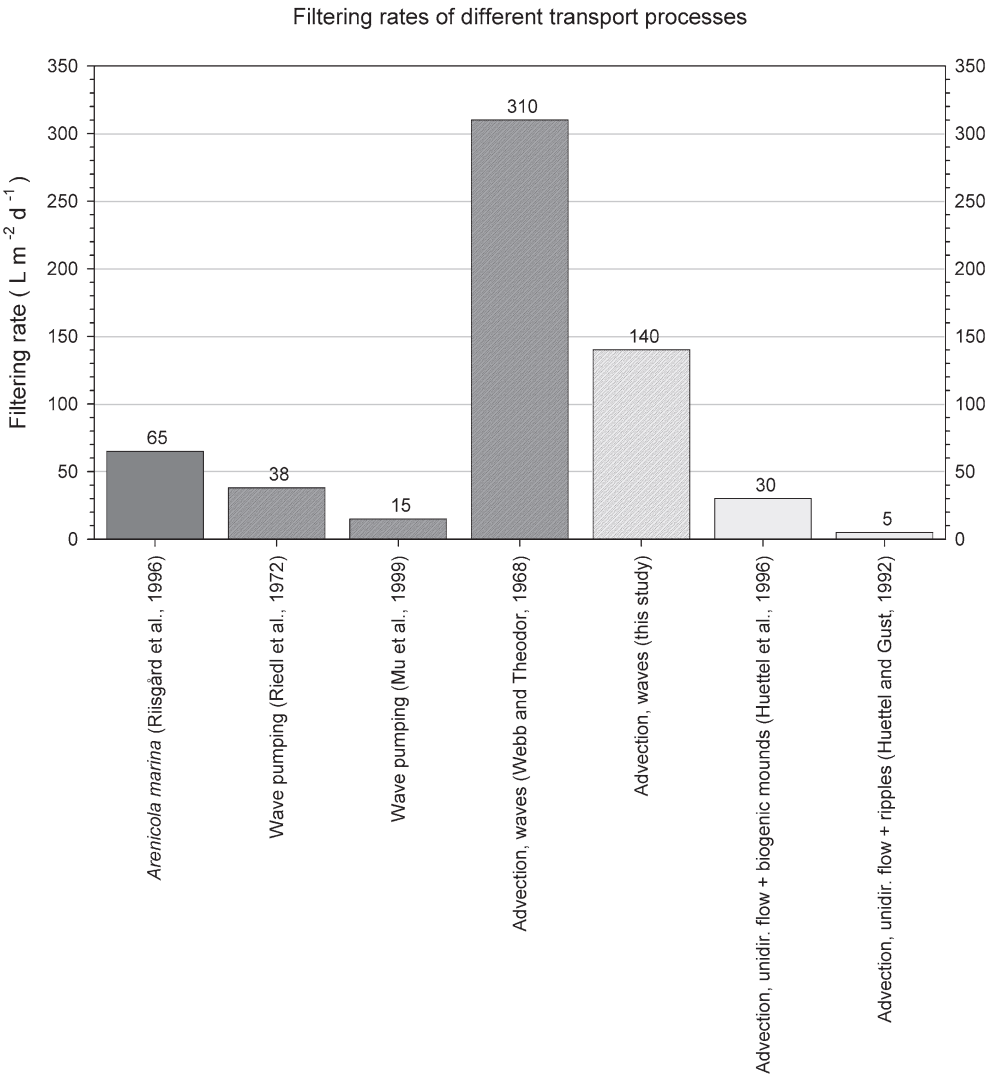

Fig. 9. Comparison of filtering rates through permeable sediments driven by different processes (Riisgård et al., 1996; Mu et al., 1999).

the filtration caused by wave - sediment topography - interaction is the efficient transport of organic substances and electron acceptors into the sands, thereby increasing the contribution of per-meable sediments in the coastal mineralisation of matter.

Future research should attempt to assess pore water velocities under variable wave conditions, water depths and sediment characteristics in order to quantify the contribution of wave-related sediment filtration to the coastal cycles of matter.

Acknowledgements

We thank Prof. B.B. Jørgensen for his interest and support in this work. We especially would like to acknowledge H. Røy for his help and constructive ideas during fieldwork. We appreciate the co-operation of F. Janssen and C. Wild before and during the measurement campaign. J. Jensen is thanked for assistance during fieldwork, M. Alisch for nutrient analyses, and V. Meyer, P. Färber and

G. Herz for their help with the electronics. The careful and constructive reviews of Carlos Rocha and one anonymous reviewer are much appreciated. This study was funded by the Max Planck Society (MPG).

References

Berger, W.H., Smetacek, V.S., Wefer, G., 1989. Ocean productivity and paleoproductivity — an overview. In: Berger, W.H., Smetacek, V.S., Wefer, G. (Eds.), Productivity of the Ocean: Present and Past. John Wiley & Sons, New York, pp. 1–34.

Black, K.P., Oldman, J.W., 1999. Wave mechanisms responsible for grain sorting and non-uniform ripple distribution across two moderate-energy, sandy continental shelves. Mar. Geol. 162, 121–132.

Boudreau, B.P., 1996. The diffusive tortuosity of fine-grained unlithified sediments. Geochim. Cosmochim. Acta 60, 3139–3142.

Cacchione, D.A., Wiberg, P.L., Lynch, J., Irish, J., Traykovski, P., 1999. Estimates of suspended-sediment flux and bedform activity on the inner portion of the Eel continental shelf. Mar. Geol. 154, 83–97.

Canfield, D.E., Teske, A., 1996. Late proterozoic rise in atmospheric oxygen concentration inferred from phylogenetic and sulphur-isotope studies. Nature 382, 127–132.

De Beer, D., Schramm, A., 1999. Micro-environments and mass transfer phenomena in biofilms studied with microsensors. Wat. Sci. Tech. 39, 173–178.

De Haas, H., Van Weering, T.C.E., De Stigter, H., 2002. Organic carbon in shelf seas: sinks or sources, processes and products. Cont. Shelf Res. 22, 691–717.

Durrieu De Madron, X., Abassi, A., Heussner, S., Monaco, A., Aloisi, J.C., Radakovitch, O., Giresse, P., Buscail, R., Kerherve, P., 2000. Particulate matter and organic carbon budgets for the Gulf of Lions (NW Mediterranean). Oceanol. Acta 23, 717–730.

Elliott, A.H., 1990. Transfer of solutes into and out of streambeds. Ph.D. Thesis, California Institute of Technology, Pasadena.

Elliott, A.H., Brooks, N.H., 1997a. Transfer of nonsorbing solutes to a streambed with bed forms: Theory. Water Resour. Res. 33, 123–136.

Elliott, A.H., Brooks, N.H., 1997b. Transfer of nonsorbing solutes to a streambed with bed forms: Laboratory experiments. Water Resour. Res. 33, 137–151.

Emery, K.O., 1968. Relict sediments on continental shelves of the world. Am. Assoc. Pet. Geol. Bull. 52, 445–464.

Eylers, H., Brooks, N.H., Morgan, J.J., 1995. Transport of adsorbing metals from stream water to a stationary sand-bed in a laboratory flume. Mar. Freshw. Res. 46, 209–214.

Grasshoff, K., Kremling, K., Ehrhardt, M., 1999. Methods of Seawater Analysis. Wiley-VCH Verlag, Weinheim.

Harrison, W.D., Musgrave, D., Reeburgh, W.S., 1983. A wave-induced transport process in marine sediments. J. Geophys. Res. 88, 7617–7622.

Huettel, M., Gust, G., 1992. Impact of bioroughness on interfacial solute exchange in permeable sediments. Mar. Ecol. Prog. Ser. 89, 253–267.

Huettel, M., Rusch, A., 2000. Transport and degradation of phytoplankton in permeable sediment. Limnol. Oceanogr. 45, 534–549.

Huettel, M., Webster, I.T., 2001. Porewater flow in permeable sediments. In: Boudreau, B.P., Jørgensen, B.B. (Eds.), The Benthic Boundary Layer. Oxford University Press, Oxford, pp. 144–179.

Huettel, M., Ziebis, W., Forster, S., 1996. Flow-induced uptake of particulate matter in permeable sediments. Limnol. Oceanogr. 41, 309–322.

Huettel, M., Ziebis, W., Forster, S., Luther, G.I., 1998. Advective transport affecting metal and nutrient distribution and interfacial fluxes in permeable sediments. Geochim. Cosmochim. Acta 62, 613–631.

Hutchinson, P.A., Webster, I.T., 1998. Solute uptake in aquatic sediments due to current-obstacle interactions. J. Environ. Eng.-ASCE 124, 419–426.

Jørgensen, B.B., 2001. Life in the diffusive boundary layer. In: Boudreau, B.P., Jørgensen, B.B. (Eds.), The Benthic Boundary Layer. Oxford University Press, Oxford, pp. 348–373.

Klimant, I., Meyer, V., Kühl, M., 1995. Fiber-optic oxygen microsensors, a new tool in aquatic biology. Limnol. Oceanogr. 40, 1159–1165.

Klute, A., Dirksen, C., 1986. Hydraulic conductivity and diffusivity: laboratory methods. In: Klute, A. (Ed.), Methods of Soil Analysis — Part 1 — Physical and Mineralogical Methods. Am. Soc. Agron, Madison, WI, pp. 687–734.

Krögel, F., 1997. Einfluß von Viskosität und Dichte des Seewassers auf Transport und Ablagerung von Wattsedimenten (Langeooger Rückseitenwatt, südliche Nordsee). Ber. aus d. FB Geow. d. Univ. Bremen 102, 168 pp.

Li, L., Barry, D.A., Stagnitti, F., Parlange, J.Y., 1999. Submarine groundwater discharge and associated chemical input to a coastal sea. Water Resour. Res. 35, 3253–3259.

Li, M.Z., Amos, C.L., 1999. Field observations of bedforms and sediment transport thresholds of fine sand under combined waves and currents. Mar. Geol. 158, 147–160.

Li, Y.H., Gregory, S., 1974. Diffusion of ions in sea water and in deep sea sediments. Geochim. Cosmochim. Acta 38, 703–714.

Lohse, L., Epping, E.H.G., Helder, W., Van Raaphorst, W., 1996. Oxygen pore water profiles in continental shelf sediments of the North Sea - turbulent versus molecular diffusion. Mar. Ecol. Prog. Ser. 145, 63–75.

Longuet-Higgins, M.S., 1983. Wave set-up, percolation and undertow in the surf zone. Proc. R. Soc. London Ser. A-Math. Phys. Eng. Sci. 390, 283–291.

Mu, Y.K., Cheng, A.H.D., Badiey, M., Bennett, R., 1999. Water wave driven seepage in sediment and parameter inversion based on pore pressure data. Int. J. Numer. Anal. Methods Geomech. 23, 1655–1674.

Nielsen, P., 1990. Tidal dynamics of the water-table in beaches. Water Resour. Res. 26, 2127–2134.

Ohara, S.C.M., Dando, P.R., Schuster, U., Bennis, A., Boyle, J.D., Chui, F.T.W., Hatherell, T.V.J., Niven, S.J., Taylor, L.J., 1995.

Gas seep induced interstitial water circulation — observations and environmental implications. Cont. Shelf Res. 15, 931–994.
Precht, E., Huettel, M., 2003. Advective pore water exchange driven by surface gravity waves and its ecological implications. Limnol. Oceanogr. 48, 1674–1684.
Riedl, R.J., Machan, E.A., 1972. Hydrodynamic patterns in lotic intertidal sands and their bioclimatological implications. Mar. Biol. 13, 179–209.
Riedl, R.J., Huang, N., Machan, R., 1972. The subtidal pump: a mechanism of interstitial water exchange by wave action. Mar. Biol. 13, 210–221.
Riisgård, H.U., Berntsen, I., Tarp, B., 1996. The lugworm (*Arenicola marina*) pump: characteristics, modelling and energy cost. Mar. Ecol. Prog. Ser. 138, 149–156.
Rocha, C., 2000. Density-driven convection during flooding of warm, permeable intertidal sediments: the ecological importance of the convective turnover pump. J. Sea Res. 43, 1–14.
Rusch, A., Forster, S., Huettel, M., 2001. Bacteria, diatoms and detritus in an intertidal sandflat subject to advective transport across the water-sediment interface. Biogeochemistry 55, 1–27.
Rutgers van der Loeff, M.M., 1981. Wave effects on sediment water exchange in a submerged sand bed. Neth. J. Sea Res. 15, 100–112.
Savant, S.A., Reible, D.D., Thibodeaux, L.J., 1987. Convective transport within stable river sediments. Water Resour. Res. 23, 1763–1768.
Shum, K.T., 1992. Wave-induced advective transport below a rippled water-sediment interface. J. Geophys. Res. 97, 789–808.
Shum, K.T., 1993. The effects of wave-induced pore water circulation on the transport of reactive solutes below a rippled sediment bed. J. Geophys. Res. 98, 10289–10301.
Shum, K.T., Sundby, B., 1996. Organic matter processing in continental shelf sediments — the subtidal pump revisited. Mar. Chem. 53, 81–87.
Thibodeaux, L.J., Boyle, J.D., 1987. Bedform-generated convective transport in bottom sediment. Nature 325, 341–343.
Turner, I.L., Masselink, G., 1998. Swash infiltration-exfiltration and sediment transport. J. Geophys. Res. Oceans 103, 30813–30824.
Webb, J.E., Theodor, J., 1968. Irrigation of submerged marine sands through wave action. Nature 220, 682–683.
Webb, J.E., Theodor, J.L., 1972. Wave-induced circulation in submerged sands. J. Mar. Biol. Assoc. UK 52, 903–914.
Webster, I.T., Norquay, S.J., Ross, F.C., Wooding, R.A., 1996. Solute exchange by convection within estuarine sediments. Estuar. Coast. Shelf Sci. 42, 171–183.
Webster, I.T., Taylor, J.H., 1992. Rotational dispersion in porous-media due to fluctuating flows. Water Resour. Res. 28, 109–119.
Ziebis, W., Huettel, M., Forster, S., 1996. Impact of biogenic sediment topography on oxygen fluxes in permeable seabeds. Mar. Ecol. Prog. Ser. 140, 227–237.